



Effective Stiffness and Damping Analysis of Steel Damper to Lateral Cyclic Loading

Bastian A. Ampangallo ^{1*}, Herman Parung ¹, Rita Irmawaty ¹, Arwin Amiruddin ¹

¹Department of Civil Engineering, Faculty of Engineering, Hasanuddin University, South Sulawesi 91711, Indonesia.

Received 21 March 2024; Revised 25 May 2024; Accepted 07 June 2024; Published 01 July 2024

Abstract

Steel dampers are components used in building structures to reduce vibration and energy generated by dynamic loads such as earthquakes. Several factors affect the effectiveness of steel dampers in reducing energy, including the cross-sectional area, mass distribution, cross-sectional geometry, and material stiffness. The cross-sectional geometry or shape of the steel damper can affect how energy is absorbed and dissipated in the structural system. Cross sections with different geometric variations can have different mechanical responses to dynamic loads. This study aims to analyze which type of steel damper is effective in terms of stiffness and damping capacity against lateral cyclic loads. The steel damper cross-sectional variations used are slit steel dampers (SSDs), tapered steel dampers (TSDs), and oval steel dampers (OSDs). Cyclic testing of the dampers used displacement control with the same target deviation for all three damper types. The results showed that the stress and strain distributions of the oval steel damper were more even than those of the other two models. The variations in the energy dissipation capacities of the three cross-section variations are relatively the same. However, the slit steel damper type has the best stiffness compared to the other two types. This research is ultimately expected to influence the science of the structure of a building in preventing and anticipating earthquakes or other disasters.

Keywords: Energy Dissipation; Lateral Cyclic Loading; Steel Damper; Strain Distribution.

1. Introduction

Earthquakes are among the deadliest natural disasters that cause emotional, social, and financial losses [1, 2]. In the last ten years, several earthquakes have caused considerable loss of life and damage [3]. Reuters' news agency has recorded several earthquake events in the past decade across the hemisphere, including the Sichuan Earthquake in China in 2013. An earthquake measuring 7.0 on the Richter Scale shook China's Sichuan province. It has caused significant damage and killed approximately 200 people. Thousands of people were also injured. More than 8,000 people were killed, and millions more were affected by this earthquake. In 2017, Mexico City and its surroundings were rocked by an earthquake measuring 7.1 on the Richter Scale. This earthquake caused severe damage and killed more than 360 people.

In July and August 2018, the Indonesian island of Lombok, Indonesia, was rocked by a series of high-magnitude earthquakes. The strongest earthquake had a magnitude of 6.9 on the Richter scale. These earthquakes caused extensive damage, killed more than 500 people, and displaced thousands of residents. On September 28, 2018, Central Sulawesi, Indonesia, was hit by a 7.5 magnitude earthquake followed by a tsunami. This disaster devastated the city of Palu and its surroundings, killing more than 4,300 people and leaving thousands more of people missing or injured.

With respect to the response of structures subjected to dynamic loads, such as earthquakes, the energy generated by these dynamic loads can cause excessive vibration and damage the structure [4]. This dynamic response can physically

* Corresponding author: ampangalloba21d@student.unhas.ac.id

<http://dx.doi.org/10.28991/CEJ-2024-010-07-017>



© 2024 by the authors. Licensee C.E.J, Tehran, Iran. This article is an open access article distributed under the terms and conditions of the Creative Commons Attribution (CC-BY) license (<http://creativecommons.org/licenses/by/4.0/>).

damage the structure and threaten human safety [5]. Scientists have performed much research and provided several alternatives to reduce and even prevent damage to structures caused by earthquakes [6]. One of the alternatives proposed is the application of structural control systems that can increase the seismic capacity of structural systems in the form of dampers on structural elements [7]. The installed control system dissipates the earthquake energy entering the structural system. These control systems are better known as seismic devices [8]. In general, this structural control system works by changing the stiffness and adding mass to the structure so that when an earthquake occurs, the structural elements can be controlled and planned in an elastic state [9].

The category of passive control systems (passive energy dissipation devices) is grouped based on the energy dissipation mechanism, which consists of base isolators, viscoelastic devices, tuned mass dampers, metallic yielding dampers, friction dampers, liquid dampers, and viscous dampers [10, 11]. A metallic damper or metallic yielding damper is a steel material used as a passive energy dissipator in planning an earthquake-resistant building [12]. Metallic dampers dissipate incoming energy through inelastic deformation of the material [13]. This device is less expensive than other dissipation devices, and its installation is simple. It is installed on the structure to reduce the deformation due to earthquake forces through the inelastic deformation of the damper, where this passive control system has elastic stiffness [14]. Using this damper minimizes the response of structural deviation and stops vibration so that the deviation between levels can be minimized and the lateral force of the column becomes small [15].

The difference in mechanism also economically affects the choice of damper installation model [16]. Installation in the weak-axis direction requires more dampers and is, therefore, more expensive than installation in the strong-axis direction [17]. Dampers installed in the direction of shear force have much greater stiffness [18].

The mechanism and damping capacity of metallic dampers depend on the materials used, such as steel, aluminum, copper, and tin [19]. Several recent studies have been conducted to obtain a suitable steel damper design. Hwang et al. [20] conducted low-cycle fatigue tests on slit dampers with different strip configurations. The test results showed that the energy dissipation capacity of the slit damper was quite good, but the damper suffered a brittle failure. Furthermore, Feng et al. [21] continued their research to identify the cause of brittle failure. The researchers suggested that the brittle failure that occurred in the strip model slit damper was caused by the stress concentration accumulated at the end of the blades/strips of the damper. Therefore, researchers have optimized the blade shape of slit steel dampers.

Bae et al. [22] researched three different steel strip damper models (barbell-shaped, tapered, and hourglass-shaped strips). All three models exhibited increased capacity under cyclic loading, stable hysteretic behavior, and cracks distributed along the blade/strip. Kim & Kim [23] developed a damper model composed of four steel plates with different configurations where each end of the blade was curved to minimize stress concentration. The results of the experimental study showed very stable hysteretic behavior.

The research by Bae et al. and Kim & Kim was further developed by Liu et al. [24] by performing a numerical analysis to obtain the optimal shape of the damper by considering the height-to-width ratio. Researchers have modeled three damper models (steel slit dampers) with the same model parameters but with different cross-sectional height variations. This research concluded that by reducing the width at the center of the cross-section (slit), brittle failure due to stress concentration at the end region of the strip can be avoided. The effective damping of the tested dampers is in the range of 10%-25%, and the increase in the damping capacity of the test specimens occurs at damper heights between 90 and 270 mm.

In this study, experimental testing was conducted on three types of steel dampers (slit steel dampers, tapered steel dampers, and oval steel dampers) with different opening type variations, for which two damper geometry models were used according to previous research. The difference in the shape of the opening (slit) is a distinguishing factor from previous research. The shape of the slit in the steel damper studied is oval. The oval shape of the steel damper slit is selected by assuming that the stress distribution along the strip of the damper will be more even. The steel material used to manufacture the damper is a steel plate. Tensile tests (coupon tests) were carried out to determine the characteristics of the steel plate material according to the American Standard Testing and Materials (ASTMs).

2. Method

2.1. Test Specimen Design

The test specimen samples to be studied are made of steel plate base material. The type of steel plate used is structural steel grade 400 (structural steel 400). The reason for choosing this type of steel plate is that, in addition to being inexpensive, this type of steel is also readily available on the market. As shown in Figure 2, the planned damper has dimensions of 500 mm long, 360 mm high, and 10 mm thick. Nine SG1-SG9 strain gauges are installed on the top of the cross section of the damper cross section to ensure that strains occur. Stress concentration occurs at the edges of the damper, which causes brittle failure. Strain gauges installed on the end and middle sides of the damper are used to determine the stress and strain distributions that occur in the damper and to observe the stress concentration.

Three types of samples were tested, namely slit steel dampers (SSDs), tapered steel dampers (TSDs), and oval steel dampers (OSDs). The geometry dimensions are presented in Table 1.

Table 1. Dimensions of the specimens

Sample's Name	Length (w/mm)	Height (H/mm)	Slit Height (h/mm)	Thickness (t/mm)	Center Section Width (bc/mm)
SSD	550	360	180	10	36
TSD	500	360	180	10	16
OSD	500	360	180	10	16

Modeling using finite element methods was performed to validate the experimental test results. The damping capacity of the damper is expressed in terms of the effective stiffness (K_{eff}) and effective damping (β_{eff}), from which the following equations can be obtained.

$$K_{eff} = \frac{|P_{max}| + |P_{min}|}{|\delta_{max}| + |\delta_{min}|} \tag{1}$$

$$\beta_{eff} = \frac{2}{\pi} \frac{E_{loop}}{K_{eff}(|\delta_{max}| + |\delta_{min}|)} \tag{2}$$

where P_{max} and P_{min} are the maximum and minimum loads, δ_{max} and δ_{min} are the maximum and minimum displacements, respectively, and E_{loop} is the dissipated energy per cycle.

The parameters needed to obtain the stiffness and damping values are obtained from the damping and stiffness characteristics, as shown in Figure 1.

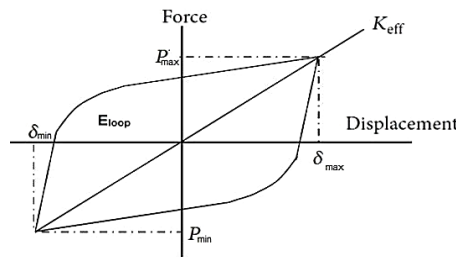


Figure 1. Damping and stiffness characteristics

Three damper variations, namely, tapered steel dampers, oval steel dampers, and slit steel dampers, were tested to meet the research objective of analyzing the effect of cross-sectional geometry on damping effectiveness. All dampers have the same height-to-width ratio. Likewise, the thickness of the damper. The geometries of the three dampers are shown in Figure 2.

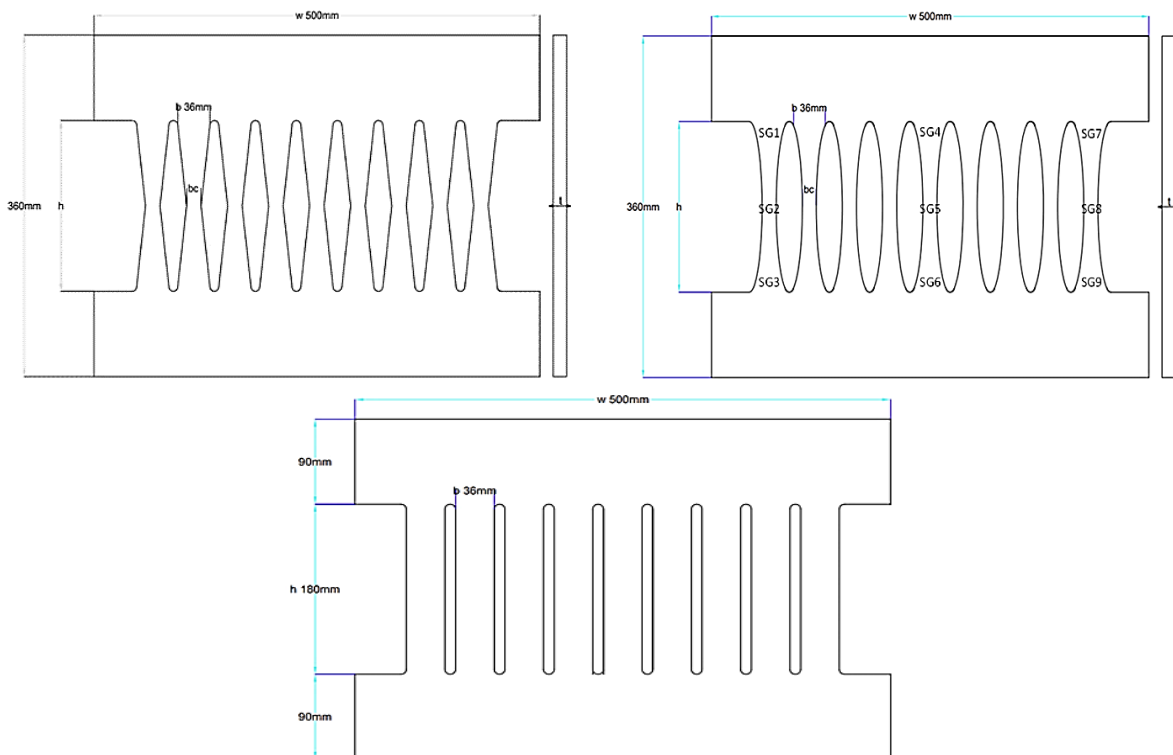


Figure 2. Damper cross-section geometry

The reference specimen is a slit steel damper. The steel material used is a structural steel plate, where a material characterization test has previously been carried out, and the steel material is included in BJ SS 400.

2.2. Test Set Up and Loading Procedure

The damper specimen to be tested is mounted on a steel portal made of IWF steel. For ease of installation and replacement of the damper before and after the test, the damper and portal were connected using bolts. Strain gauges were installed at several cross-sections of the damper to read the strain that occurred during loading. The stress and strain distributions in the damper cross-section can be determined by installing strain gauges at these points.

LVDTs were installed at several sections with the main LVDT position parallel to the actuator to read the relative displacement values. The LVDT parallel to the actuator was used for the data.

2.3. Damper Plate Characteristics

The material used for the damper is a grade 400 structural steel plate (SS 400). In this study, a characteristic test in the form of a steel plate tensile test was first performed for each type of damper studied (Table). The thickness of the plate used in this study is 10 mm.

Table 2. Test results of the steel plate characteristics

Sample Type	Melting (MPa)	Tensile (MPa)	Melt Ratio (%)	Elongation (%)
1	288.293	404.390	71.29	15.91
2	280.976	401.951	69.90	17.05
3	268.780	404.390	66.47	18.18

2.4. Model for Testing the Damper

Cyclic testing of the damper used displacement control with the same target deviation for the three types of dampers, namely 2 mm (0.5 Δ), 4 mm (1 Δ), 8 mm (2 Δ), 12 mm (3 Δ), 16 mm (4 Δ), 20 mm (5 Δ), 24 mm (6 Δ), 28 mm (7 Δ), 32 mm (8 Δ), 36 mm (9 Δ), 40 mm (10 Δ), and 48 mm (12 Δ). During the test, a data logger connected to the cyclic tester recorded the load, deviation, and strain. There were nine strain gauges on each damper sample. The placement of the strain gauges used to measure the strain is shown in Figure 3.

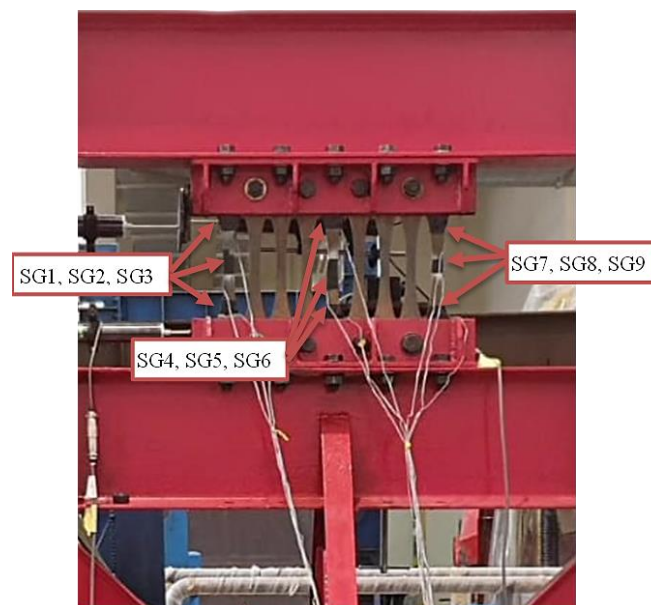


Figure 3. Test set up

The anvil is connected to the strong floor using bolts. Strain gauges were installed on 12 damper parts for each variation. Each point is marked sequentially, starting from SG1 to SG12. The aim of installing strain gauges is to read the strain in the damper when given a cyclic load. The LVDT is parallel to the actuator axis to measure displacement. The measuring instruments were then connected to a data logger to record the strain and displacement.

The foundation/mount of the damper is a frame that is placed parallel to the axis of the actuator. The damper to be tested is then mounted on the frame and connected using bolts. The test setup is shown in Figure 4.

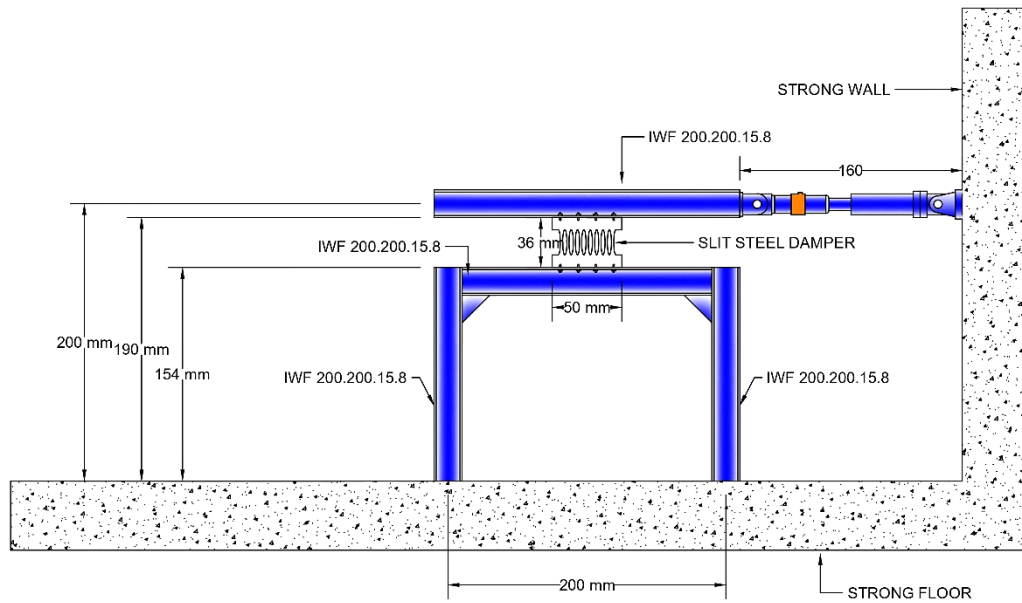


Figure 4. Setup cyclic testing

2.5. Research Flowchart

The conclusions that can be drawn from the method used are available in Figure 5.

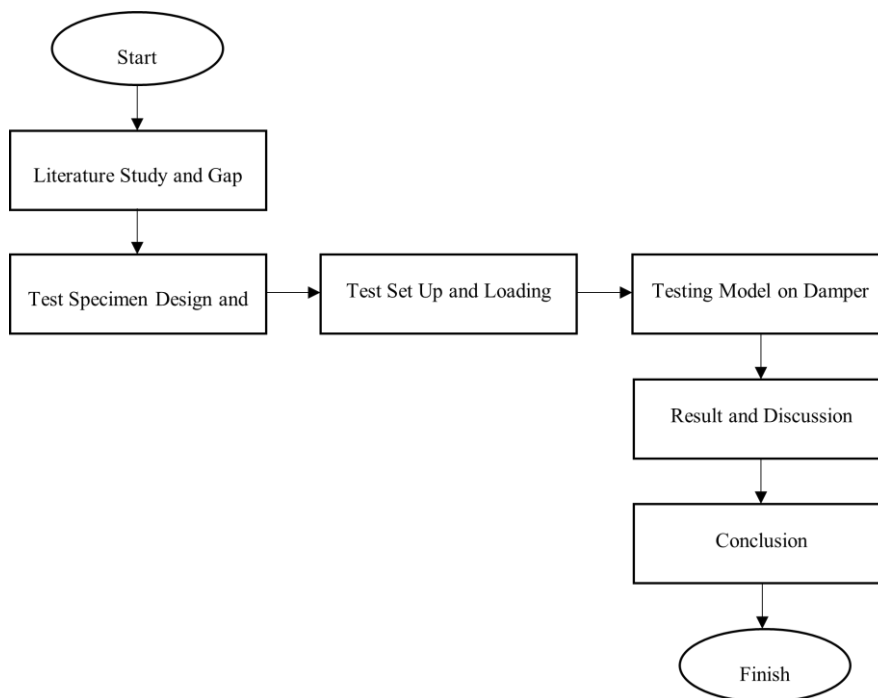


Figure 5. Flowchart of the research

3. Results

3.1. Strain Distribution of Steel Dampers with Variations in the Cross-Section Opening to Lateral Cyclic Load

For the three types of samples tested under cyclic loading, at minor deviations, there is no visible change in the shape of the damper. However, when the deviation increases, the damper cross-section changes shape. The change in shape in question is a curved cross-section, and cracks begin to appear in the cross-section. After 12 cycles of applied loading, the damper appears deformed, but no damage is visible. This indicates that the damper has good strength.

The strain distribution of the OSD-type damper is shown in Figure 6. The figure shows that the maximum strain in the oval-type damper is 429.70 $\mu\epsilon$. As shown in Table 3, the maximum strain occurs at position SG 7 in the cross-section. Overall, the strain values are relatively the same for the upper side (SG 1, SG 4, and SG 7) for the cross-sections on the middle and lower sides.

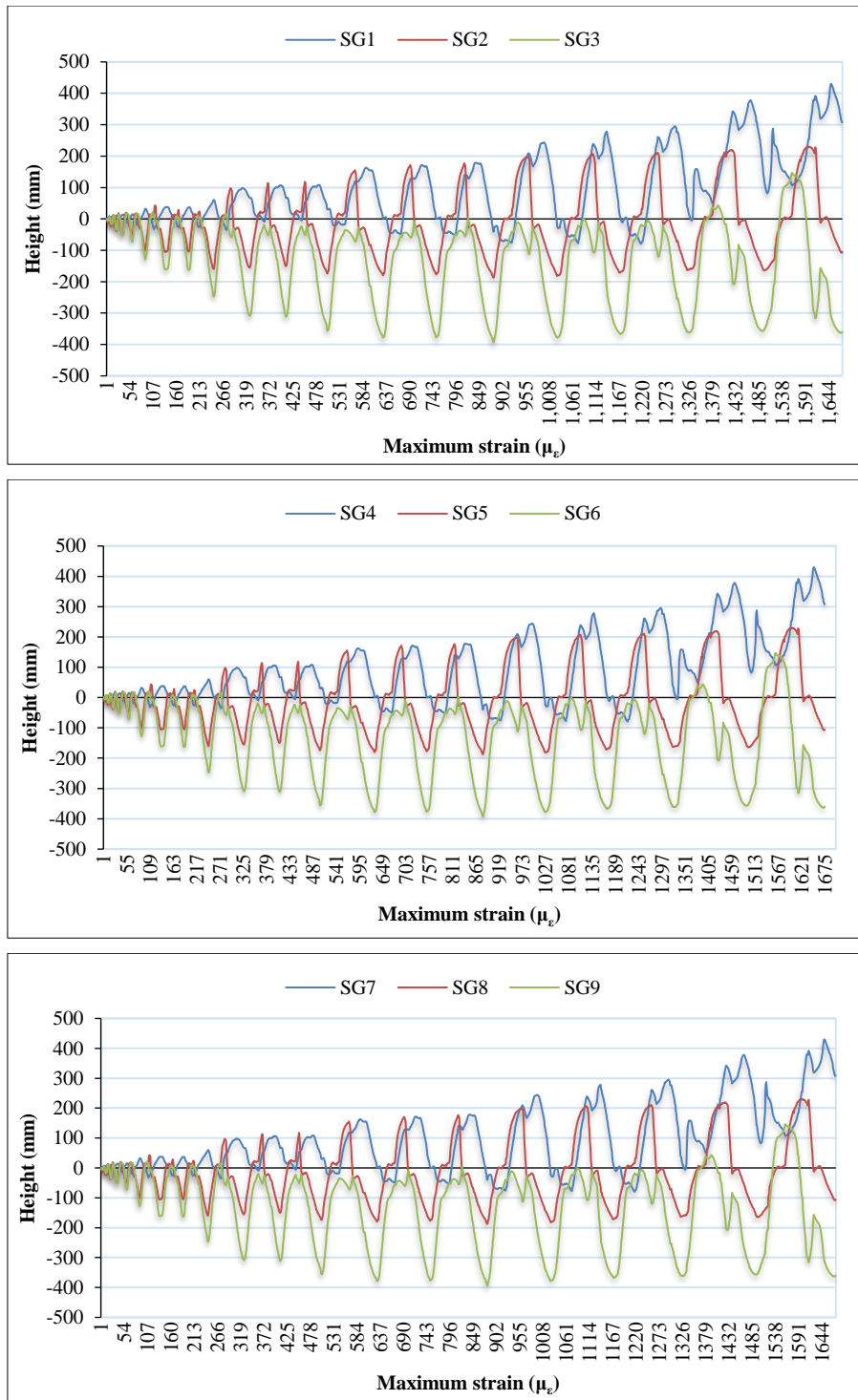


Figure 6. Strain graph of the oval steel damper

Table 3. Strain based on experimental testing for the OSD type

Cross-Section	Position	Strain Value (μ_e)
Top	SG 1	429.67
	SG 4	429.68
	SG 7	429.70
Middle	SG 2	229.67
	SG 8	229.69
Bottom	SG 3	146.41
	SG 6	146.44
	SG 9	146.42

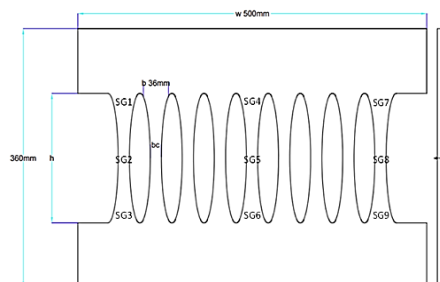


Table 4 and Figure 7 show the strain values on the tapered steel damper where the maximum strain was 397.04 $\mu\epsilon$, and the lowest strain was 141.73 $\mu\epsilon$.

Table 4. TSD-types strain based on experimental testing

Cross-Section	Position	Strain Value ($\mu\epsilon$)
Top	SG 1	397.01
	SG 4	397.02
	SG 7	397.04
Middle	SG 2	228.06
	SG 5	228.06
	SG 8	228.08
Bottom	SG 3	141.73
	SG 6	141.76
	SG 9	141.74

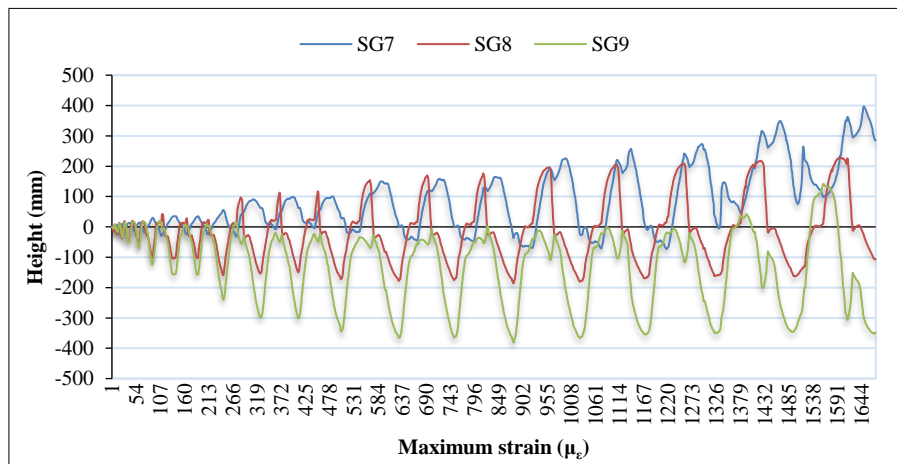
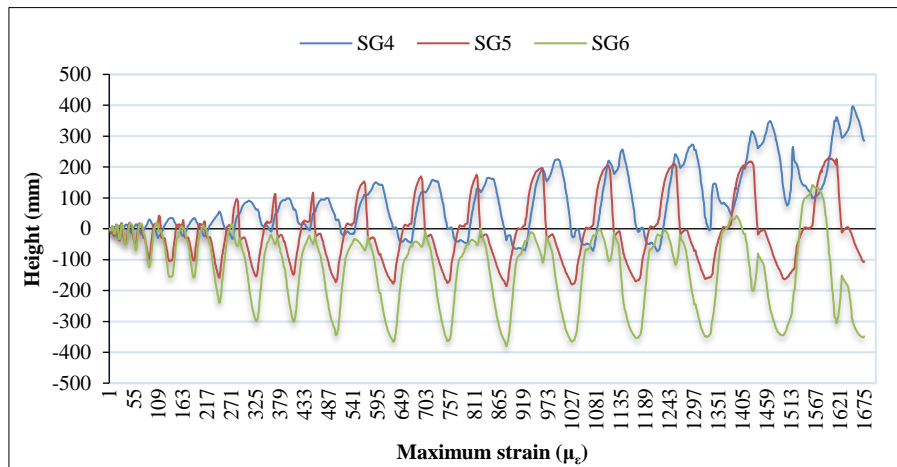
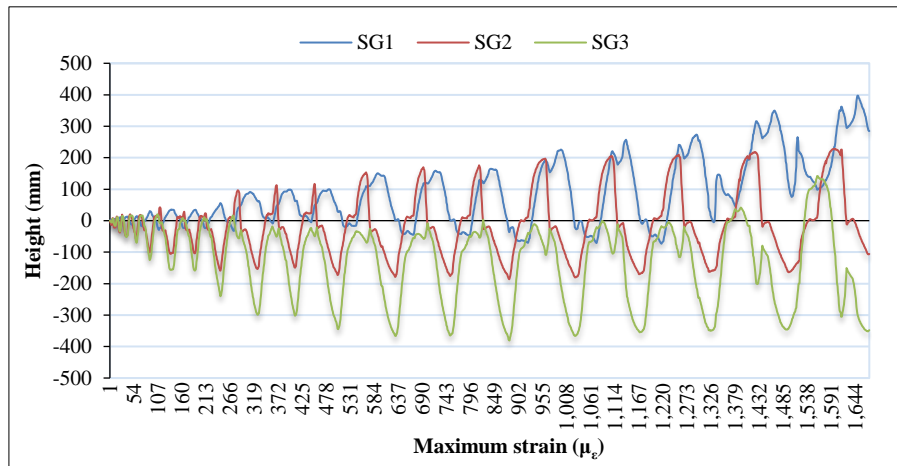
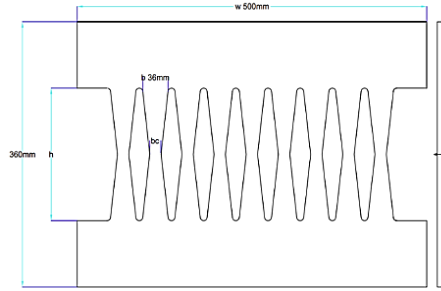


Figure 7. Strain graph of the tapered steel damper

Similar to the oval steel damper, the most prominent strain position in the tapered steel damper is at SG 7, and the smallest strain is at SG 3. The strain distribution model in this damper type is also almost the same as that in the previous damper type, where the most significant strain is on the upper side, and the least minor strain is on the lower side. In the slit steel damper (SSD) type, the strains that occur are minor compared to those of the previous two damper types. The maximum strain for the slit steel damper type is 334.31 $\mu\epsilon$, and the most minor strain is 174.32 (see Table 5).

Table 5. Strain based on experimental testing for SSD type

Cross-Section	Position	Strain Value ($\mu\epsilon$)
Top	SG 1	334.28
	SG 4	334.29
	SG 7	334.31
Middle	SG 2	174.32
	SG 5	174.34
	SG 8	174.34
Bottom	SG 3	112.59
	SG 6	112.62
	SG 9	112.60

The greatest strain occurs in the OSD-type damper. The position of the maximum strain in the three dampers occurs at the same point, namely, at SG7. The cross-sectional area influences the difference in strain among the three dampers. When the cross-sectional area of the damper is large, the area available to withstand stress also increases, which means that the stress generated in the damper decreases. When the stress is lower, the resulting strain on the damper will be minor according to Hooke's law. Therefore, when the cross-sectional area of the OSD-type damper is smaller than that of the other two damper types, the strain generated in the damper tends to increase.

3.2. Effectiveness of the Energy Dissipation of Steel Damper with Variations in the Openings in the Cross-Section against Lateral Cyclic Loads

After cyclic loading, the data logger recorded several parameters, including the load and displacement. Furthermore, the envelope curve of the specimen, which is the relationship between the force and maximum load, is given in Figure 8. The results of the maximum load and maximum displacement, which illustrate the force and displacement capacity for each specimen variation, are given in Table 6.

Table 6. Load and displacement of the test specimens for 12 loading cycles

OSD		TSD		SSD	
P (kN)	δ (mm)	P (kN)	δ (mm)	P (kN)	δ (mm)
60.593	35.420	73.143	33.340	91.249	30.210
84.949	28.830	99.673	28.570	113.265	21.320
78.848	21.600	92.514	21.370	105.130	21.330
72.356	16.000	84.898	16.760	96.475	17.140
62.426	10.400	73.247	11.750	83.235	11.910
39.113	5.880	45.892	5.540	52.150	5.550
20.993	3.100	24.631	2.740	27.990	2.630
15.908	2.380	18.665	2.070	21.210	1.980
11.003	1.580	12.910	1.380	14.670	1.310
6.210	0.900	7.286	0.760	8.280	0.730
3.094	0.340	3.630	0.370	4.120	0.340
0.000	0.000	0.000	0.000	0.000	0.000
2.554	0.200	2.996	0.260	3.405	0.270
3.881	0.340	4.554	0.510	5.175	0.500
5.288	1.060	6.204	1.100	7.050	1.040
15.908	1.700	18.665	1.590	21.210	1.540
20.993	2.440	24.631	2.140	27.990	2.180
39.113	5.020	45.892	4.200	52.120	4.420
62.426	10.680	73.247	9.910	83.235	10.300
72.356	16.000	84.898	15.330	96.475	15.770
78.848	21.660	92.514	20.660	105.130	21.640
84.949	26.740	99.673	25.580	113.265	25.879
60.953	34.880	73.143	32.270	91.429	30.366

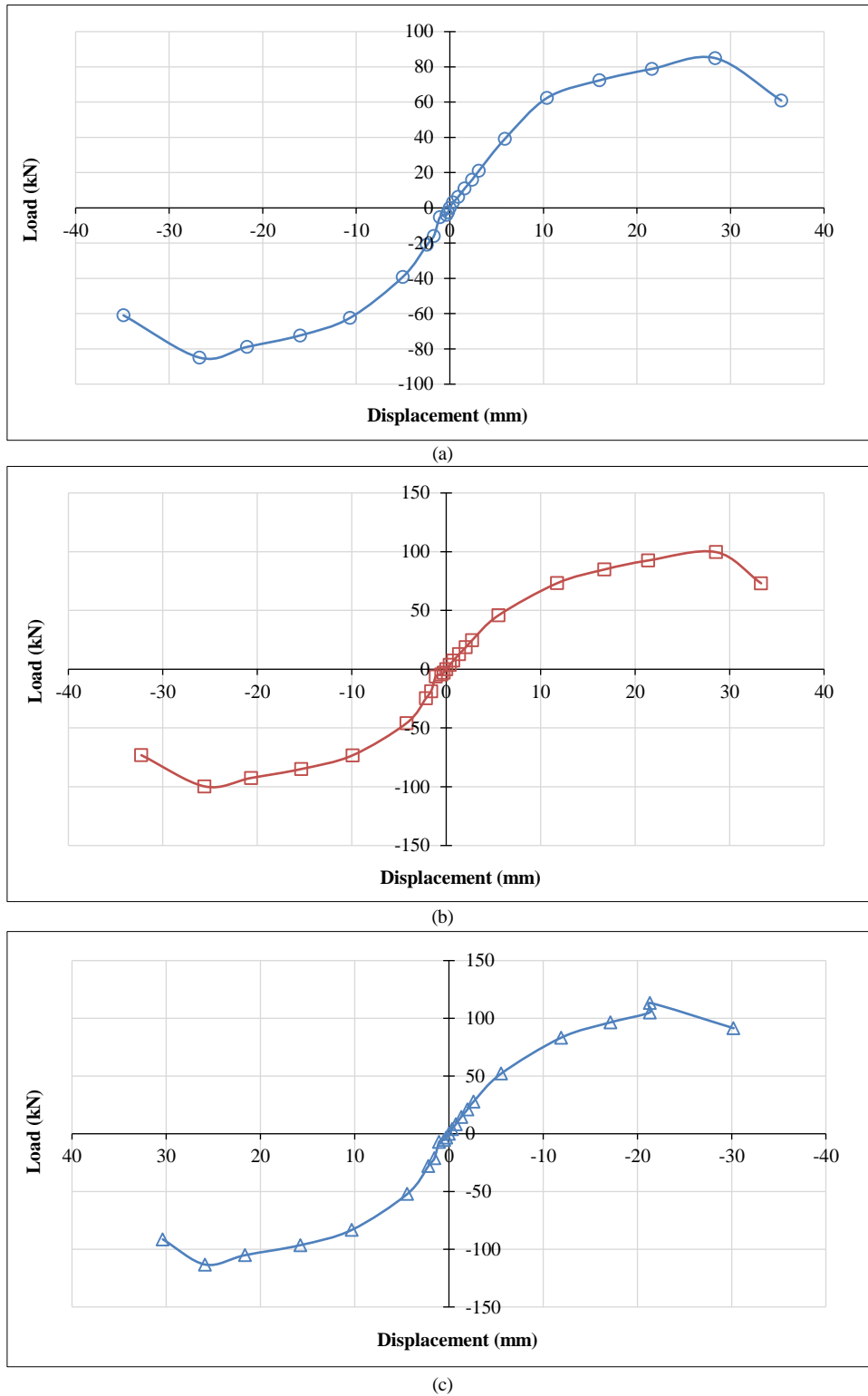


Figure 8. Envelope curves of the tested specimens (a) OSD (b) TSD (c) SSD

The difference in damper cross-sectional geometry affects the load capacity and displacement due to cyclic loading. Based on the table above, the damper with an oval cross-section (oval steel damper) has the most significant displacement. The displacement of the OSD sample is 8.52% greater than that of the slit steel damper and 1.67% greater than that of the tapered steel damper. For the load capacity, the oval cross-section decreases compared to the other two cross-section variations. The OSD has a load capacity that is 1.84% lower than that of the slit steel damper and 0.82% lower than that of the tapered steel damper. In general, reducing the cross-sectional area causes a decrease in the load capacity of the steel damper. However, the percentage decrease in the three damper variations due to the cross-sectional area reduction is insignificant.

The effective stiffness is used to calculate the potential energy at each cycle of the damper. Based on Equation 1, the variation in the effective stiffness of each test specimen at the peak load is presented in Table 7.

Table 7. Effective Stiffness

OSD		TSD		SSD	
δ (mm)	K_{eff}	δ (mm)	K_{eff}	δ (mm)	K_{eff}
35.420	1.734	33.340	2.230	30.210	3.109
28.830	3.082	28.570	3.681	21.320	4.799
21.600	3.645	21.370	4.402	21.330	4.893
16.000	4.522	16.760	5.291	17.140	5.863
10.400	5.923	11.750	6.033	11.910	7.495
5.880	6.027	5.540	6.648	5.550	7.886
3.100	6.312	2.740	6.987	2.630	8.246
2.380	6.770	2.070	7.025	1.980	8.552
1.580	7.883	1.380	7.707	1.310	9.243
0.900	8.138	0.760	9.323	0.730	10.939
0.340	10.458	0.370	10.518	0.340	12.344
0.000	0.000	0.000	0.000	0.000	0.000

The Table above shows that the SSD-type sample has the best stiffness compared to the other two damper variations at 12.344 kN/mm. For the OSD and SSD types, there is no significant difference in the stiffness; in other words, the effect of reducing the cross-sectional area ratio on changing the effective stiffness of the OSD-type damper is relatively small. The graph in Figure 9 shows that when the sample melts, the effective stiffness decreases. The change in effective stiffness at smaller displacements is significant and tends to have a steep curve, while at larger displacements, the displacement curve becomes gentler. Figure 8 also shows that the SSD-type damper has the most effective stiffness compared to the other two dampers. However, the sizeable effective stiffness does not directly affect energy absorption because the energy absorption in a damper depends more on how the damper dissipates the energy.

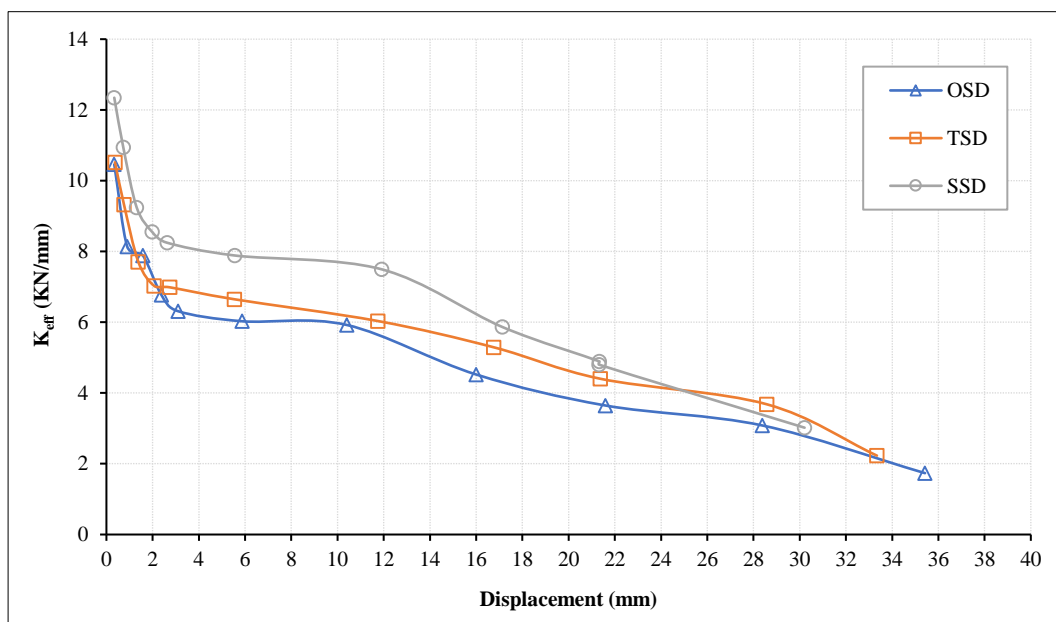


Figure 9. Effective stiffness of the test specimen

Effective damping describes the energy absorption capacity of the damper, which is closely related to displacement. The effective damping of the damper for each loading cycle can be obtained using Equation 2.

The calculation results summarized in Table 8 show differences in the practical damping values for the three types of dampers in the first three loading cycles. However, when entering the fourth to the last loading cycle, the practical damping values of the three dampers are almost the same. The calculation results also show that the OSD-type damper has the most effective damping, ranging from 15.9% to 17.6%. Meanwhile, for the TSD type, the practical damping value is 11.7% - 16.6%. Although the stiffness of the SSD-type damper is greater than that of the other two damper types, the effective damping is not better than that of the OSD-type damper, which is 15.9% - 16.6%.

Table 8. Effective damping of three types of dampers

OSD			TSD			TSD		
Eloop	K _{eff}	β _{eff}	Eloop	K _{eff}	β _{eff}	Eloop	K _{eff}	β _{eff}
35.420	1.734	0.159	33.340	2.230	0.159	30.210	3.109	0.159
28.830	3.082	0.159	28.570	3.681	0.159	21.320	4.799	0.159
21.600	3.645	0.159	21.370	4.402	0.159	21.330	4.893	0.159
16.000	4.522	0.159	16.760	5.291	0.159	17.140	5.863	0.159
10.400	5.923	0.159	11.750	6.033	0.159	11.910	7.495	0.159
5.880	6.027	0.159	5.540	6.648	0.159	5.550	7.886	0.159
3.100	6.312	0.159	2.740	6.987	0.159	2.630	8.246	0.159
2.380	6.770	0.159	2.070	7.025	0.159	1.980	8.552	0.159
1.580	7.883	0.170	1.380	7.707	0.166	1.310	9.243	0.166
0.900	8.138	0.176	0.760	9.323	0.117	0.730	10.939	0.166
0.340	10.458	0.163	0.370	10.518	0.162	0.340	12.344	0.161
0.000	0.000	0.000	0.000	0.000	0.000	0.000	0.000	0.000

4. Discussion

Research on three types of dampers with different geometric cross-sectional variations, namely, oval (OSD), tapered (TSD), and slit (SSD) types, was conducted to determine the damping effectiveness of these dampers. Several research stages were carried out, from examining steel characteristics and stress-strain analysis to energy dissipation. The tensile test results for the steel plates showed that the average maximum tensile strength for the three samples tested was 404.88 N/mm². The average strain for the three samples reached 17.12%, with a yield stress of 366.83 N/mm². The failure patterns of the three types of samples show that the steel plate material can absorb energy, indicating that the tested steel plates have good ductility properties. Based on the test results, it can be concluded that the steel grade used as a damper material has almost the same level of uniformity and belongs to the BJ SS 40 category.

Strain distribution of three different types of damper cross-sections, namely, slit steel dampers (SSDs), tapered steel dampers (TSDs), and oval steel dampers (OSDs), was conducted and the results show that the most significant strain occurs in the oval steel damper type, where the strain reaches 28.5% higher than that of the slit steel damper type. This increase in strain is due to the reduction in the cross-sectional area. The tapered steel damper type also showed a more significant strain of 18.76% compared to that of the slit steel damper. Although all three types of dampers experienced deformation based on visual observation, they did not experience significant damage.

Geometric parameters such as the strip width at the center height (bc), strip height (h), and thickness (t) were selected as critical variables to reduce the stress concentration at the tip and improve the performance in terms of the effective stiffness and damping of the three types of slit dampers. Regression equations for effective stiffness and effective damping were obtained as a function of the design variables of width at the center height of the damper (bc), damper height (h), and damper thickness (t). The relationships among the effective stiffness, effective damping, and shape variables can be formulated by referring to the second-order polynomial equation.

$$Y = \beta_0 + \sum_{i=1}^n \beta_i x_i + \sum_{i=1}^n \beta_{ii} x_i^2 + \sum_{i=1}^n \beta_{ij} x_j x_i \quad (3)$$

where Y is the design parameter, and β_0 , β_i , and β_{ij} are regression coefficients obtained from experimental test results data management.

Based on the analysis of the experimental test results, a numerical analysis can then be performed to predict the effective stiffness and effective damping of the damper expressed in terms of the design parameters with regression coefficients, which are expressed as follows:

$$K_{eff} = 7.41 + 2.21A - 26.37B - 8.55C - 0.98AB + 0.41AC + 12.88BC - 1.64A^2 + 22.92B^2 + 5.07C^2 \quad (4)$$

$$\beta_{eff} = 22.72 + 0.44A - 5.62B - 4.28C + 0.44AB + 0.79AC - 7.65BC - 1.21A^2 - 9.92B^2 + 3.84C^2 \quad (5)$$

where A, B, and C are the strip width at the damper center height (bc), strip height (h), and damper thickness (t), respectively, and the second-order interaction effects are given as (A², B², C², AB, AC, and BC).

From Equations 4 and 5, it is concluded that the strip height and thickness are the most influential factors on the effective stiffness. Moreover, the strip height significantly contributes to increasing the effective damping.

5. Conclusion

Based on the study's results, the force-displacement hysteresis curves of the three damper types tend to be stable and have good energy dissipation capacity. This is evident from the condition of the test specimen that does not buckle at the maximum displacement condition. The strain distribution in the three dampers is quite good. Based on visual observation, the three dampers were deformed but not damaged. This indicates that the damper has good strength in terms of distributing strain. In terms of stiffness, the SSD-type damper has the highest stiffness. However, the OSD type has better effective damping, so increasing the stiffness does not directly increase the damping capacity of the damper.

6. Declarations

6.1. Author Contributions

Conceptualization, B.A.A.; methodology, B.A.A., H.P., R.I., and A.A.; software, B.A.A. and A.A.; validation, H.P., R.I., and A.A.; formal analysis, B.A.A.; investigation, B.A.A., H.P., R.I., and A.A.; resources, B.A.A.; data curation, B.A.A. and H.P.; writing—original draft preparation, B.A.A. and R.I.; writing—review and editing, B.A.A., H.P., R.I., and A.A.; visualization, B.A.A.; supervision, B.A.A.; project administration, B.A.A.; funding acquisition, B.A.A. All authors have read and agreed to the published version of the manuscript.

6.2. Data Availability Statement

Data sharing is not applicable to this article.

6.3. Funding

The authors received no financial support for this articles research, authorship, and/or publication.

6.4. Conflicts of Interest

The authors declare no conflict of interest.

7. References

- [1] Mavrouli, M., Mavroulis, S., Lekkas, E., & Tsakris, A. (2023). The Impact of Earthquakes on Public Health: A Narrative Review of Infectious Diseases in the Post-Disaster Period Aiming to Disaster Risk Reduction. *Microorganisms*, 11(2), 419. doi:10.3390/microorganisms11020419.
- [2] Wang, Z., & Wang, F. (2022). Well-being Effects of Natural Disasters: Evidence from China's Wenchuan Earthquake. *Journal of Happiness Studies*, 24(2), 563–587. doi:10.1007/s10902-022-00609-z.
- [3] Mavroulis, S., Ilgac, M., Tunçağ, M., Lekkas, E., Püskülcü, S., Kourou, A., Sextos, A., Mavrouli, M., Can, G., Thoma, T., Manousaki, M., & Karveleas, N. (2022). Emergency response, intervention, and societal recovery in Greece and Turkey after the 30th October 2020, MW = 7.0, Samos (Aegean Sea) earthquake. *Bulletin of Earthquake Engineering*, 20(14), 7933–7955. doi:10.1007/s10518-022-01317-y.
- [4] De Gois Silva, M. D., & Chavarette, F. R. (2024). H-hybrid control and MRD in a steel frame building subjected to excessive vibrations caused by the dynamic action of wind and earthquake. *Journal of AppliedMath*, 2(2), 451. doi:10.59400/jam.v2i2.451.
- [5] Zhang, F., Xu, Z., Yang, Y., Qi, M., & Zhang, H. (2021). Virtual reality-based evaluation of indoor earthquake safety actions for occupants. *Advanced Engineering Informatics*, 49, 101351. doi:10.1016/j.aei.2021.101351.
- [6] McBride, S. K., Smith, H., Morgoch, M., Sumy, D., Jenkins, M., Peek, L., Bostrom, A., Baldwin, D., Reddy, E., De Groot, R., Becker, J., Johnston, D., & Wood, M. (2022). Evidence-based guidelines for protective actions and earthquake early warning systems. *Geophysics*, 87(1), WA77–WA102. doi:10.1190/geo2021-0222.1.
- [7] Hejazi, F., Farahpour, H., & Ayyash, N. (2024). Seismic performance of structure equipped with a new rubber bracing damper system. *Archives of Civil and Mechanical Engineering*, 24(1). doi:10.1007/s43452-023-00845-x.
- [8] Leblouba, M., Fageeri, A., & Al-Sadoon, Z. A. (2022). A novel seismic energy dissipation device: Laboratory tests, mathematical modeling, and numerical analysis. *Soil Dynamics and Earthquake Engineering*, 162. doi:10.1016/j.soildyn.2022.107493.
- [9] Yan, L., Li, Y., Chang, W. S., & Huang, H. (2023). Seismic control of cross laminated timber (CLT) structure with shape memory alloy-based semi-active tuned mass damper (SMA-STMD). *Structures*, 57. doi:10.1016/j.istruc.2023.105093.
- [10] Almajhali, K. Y. M. (2023). Review on passive energy dissipation devices and techniques of installation for high rise building structures. *Structures*, 51, 1019–1029. doi:10.1016/j.istruc.2023.03.025.

- [11] Gkournelos, P. D., Triantafillou, T. C., & Bournas, D. A. (2021). Seismic upgrading of existing reinforced concrete buildings: A state-of-the-art review. *Engineering Structures*, 240. doi:10.1016/j.engstruct.2021.112273.
- [12] Oliaei, M., Mashhadiyan, M., & Forootan, R. (2023). Seismic Performance Evaluation of Friction Damper and Yielding Metallic Damper in Steel Frame. *Journal of Civil Engineering Researchers*, 5(3), 1–14. doi:10.61186/jcer.5.3.1.
- [13] Aljawadi, A. S., Alih, S. C., & Vafaei, M. (2021). Mechanical behaviour of metallic yielding dampers with different aspect ratios. *Latin American Journal of Solids and Structures*, 18(2), 1–10. doi:10.1590/1679-78256350.
- [14] Kim, Y. C., Lee, H. W., & Hu, J. W. (2023). Experimental performance evaluation of elastic friction damper. *Case Studies in Construction Materials*, 18, e01823. doi:10.1016/j.cscm.2023.e01823.
- [15] Prasad, B. B., Duvigneau, F., Juhre, D., & Woschke, E. (2022). Damping performance of particle dampers with different granular materials and their mixtures. *Applied Acoustics*, 200. doi:10.1016/j.apacoust.2022.109059.
- [16] Gorji Azandariani, M., Roustaa, A. M., Usefvand, E., Abdolmaleki, H., & Gorji Azandariani, A. (2021). Improved seismic behavior and performance of energy-absorbing systems constructed with steel rings. *Structures*, 29, 534–548. doi:10.1016/j.istruc.2020.11.041.
- [17] Zhang, R., Xie, J. Y., Chouery, K. E., Liu, J., Jia, L. J., Xiang, P., Zhao, X., Macrae, G. A., Clifton, G. C., Dhakal, R. P., Ramhormozian, S., & Yan, Z. (2022). Strong axis low-damage performance of rocking column-base joints with asymmetric friction connections. *Journal of Constructional Steel Research*, 191. doi:10.1016/j.jcsr.2022.107175.
- [18] Oh, S. H., & Park, H. Y. (2022). Experimental study on seismic performance of steel slit damper under additional tensile load. *Journal of Building Engineering*, 50. doi:10.1016/j.jobe.2022.104110.
- [19] Parveez, B., Jamal, N. A., Anuar, H., Ahmad, Y., Aabid, A., & Baig, M. (2022). Microstructure and Mechanical Properties of Metal Foams Fabricated via Melt Foaming and Powder Metallurgy Technique: A Review. *Materials*, 15(15), 5302. doi:10.3390/ma15155302.
- [20] Hwang, B. K., Kim, T. S., Kim, Y. J., & Kim, J. W. (2022). A comparative study on hysteretic characteristics of austenitic stainless steel and carbon steel slit dampers under cyclic loading. *Journal of Building Engineering*, 45. doi:10.1016/j.jobe.2021.103553.
- [21] Feng, S., Tagawa, H., & Chen, X. (2023). Seesaw-twisting system with cylindrical steel slit damper for vibration control of structures. *Structures*, 50, 1376–1390. doi:10.1016/j.istruc.2023.02.077.
- [22] Bae, J., Lee, C. H., Park, M., Alemayehu, R. W., Ryu, J., Kim, Y., & Ju, Y. K. (2020). Cyclic loading performance of radius-cut double coke-shaped strip dampers. *Materials*, 13(18), 3920. doi:10.3390/MA13183920.
- [23] Kim, S. W., & Kim, K. H. (2020). Evaluation of structural behavior of hysteretic steel dampers under cyclic loading. *Applied Sciences (Switzerland)*, 10(22), 1–11. doi:10.3390/app10228264.
- [24] Liu, L., Xu, Y., Zhou, F., Hu, G., Yu, L., & He, C. (2022). Multiobjective Optimization Design for a MR Damper Based on EBFNN and MOPSO. *Applied Sciences (Switzerland)*, 12(17), 8584. doi:10.3390/app12178584.